Supporting Information

Bilek et al. 10.1073/pnas.1103277108

SI Materials and Methods

Low-density polyethylene (LDPE), ultrahigh molecular weight polyethylene (UHMWPE), polytetrafluoroethylene (PTFE), polyether sulfone (PES), polyamide 6,6 (Nylon), polyvinyl chloride (PVC), and polystyrene (PS) films of 50-μm thickness were purchased from Goodfellow. Polymethylmethacrylate (PMMA) films were cast from solution in acetone/ethylacetate. PMMA beads were purchased from BASF. Medical-grade polydimethylsiloxane (PDMS) (MED-1134; thickness 0.05 in.) was supplied by NuSil Technology. Elast-Eon 2A was provided by AorTech Biomaterials Pty. Ltd. Attenuated total reflection (ATR)-FTIR spectra, X-ray photoelectron spectroscopy (XPS), and wetting measurements were used to check for surface contamination prior to use in experiments.

Horseradish peroxidise (HRP) and catalase enzymes were purchased from Sigma Aldrich. Human recombinant tropoelastin was expressed in house as described in the literature (1). Polyamino acids, blockers, and other reagents were purchased from Sigma Aldrich.

Plasma immersion ion implantation was carried out in an inductively coupled radio-frequency plasma powered at 13.56 MHz. The base pressure of the system was 10^{-6} torr (10^{-4} Pa). The pressure of nitrogen (99.999% pure) during implantation was 2×10^{-3} torr (4.4×10^{-2} Pa), and the pressure of argon (99.999%) during implantation was 0.3×10^{-3} torr (0.66×10^{-2} Pa). The flow rates were 100 standard cubic centimeters (sccm) for nitrogen and 10 sccm in the case of argon. The plasma power was 100 W with reverse power of 12 W when matched.

The samples were mounted on a stainless steel holder, with a stainless steel mesh of 150-mm diameter, electrically connected to the holder and placed 45 mm in front of the sample surface. Acceleration of ions from the plasma was achieved by the application of 20-kV high-voltage bias pulses of 20-μs duration to the sample holder at a frequency of 50 Hz, unless otherwise specified. The sample holder was earthed between the pulses. The samples were treated for durations of 20–1,600 s (800 s unless otherwise specified), corresponding to implantation ion fluence of $0.02–2.0 \times 10^{16}$ ions/cm^{-2}.

The ion fluence was calculated from the number of high-voltage pulses multiplied by the fluence corresponding to one pulse. The fluence of one high-voltage pulse was determined by comparing UV transmission spectra from polyethylene films implanted under conditions used here to samples implanted with known fluences in previous plasma immersion ion implantation (PIII) and ion beam treatment experiments.

Plasma treatment without PIII was carried out as follows. Polymer sheets were cut into 0.8 cm × 8 cm strips and wiped with 100% ethanol. Samples were mounted onto the substrate holder and immersed in the inductively coupled rf plasma; rf powers between 20 and 100 W were used with working gas pressure of 2 mtorr high-purity nitrogen (99.999%) with a flow rate of 72 sccm. The treatment time was 800 s unless stated otherwise.

Plasma polymer deposition utilizes two plasma sources: One rf electrode (bottom electrode) is driven at 13.56 MHz and 150 W through a matching network to generate plasma; the other one (top electrode) is powered by a dc pulsed voltage source, which is used for biasing the substrates. Unless stated otherwise, the pulse voltage was 200 V at 10 kHz with a duty cycle of 10%. The base pressure of the system was 1×10^{-4} Pa. Acetylene (purity 98%) was injected into the plasma chamber as the polymer precursor and mixed with argon and nitrogen unless otherwise specified. The flow of argon (99.999%) and the flow of nitrogen (99.999%) were both 4 sccm. In cases where only one of nitrogen or argon were used, its flow rate was 8 sccm. For samples containing hydrogen, the flow rates additional to acetylene were 4 sccm argon and 20 sccm hydrogen (99.999%), whereas the oxygen-containing samples were made with 0.4 sccm oxygen (99.999%) and 7.6 sccm argon. All samples were made with acetylene flow rate of 10 sccm. The gas flow rates were regulated using MKS mass flow controllers. The pressure during the deposition was 20 Pa. Substrates used included 316L stainless steel foil (25 μm thick) for ELISA and thin (12 μm thick) polyimide film from Goodfellow for electron spin resonance (ESR) measurements. All depositions were conducted without heating or cooling of the substrate. The typical surface temperature was approximately 40–50 °C measured immediately after the deposition. The temperature was only weakly dependent on the bias pulse voltage because of the small duty cycle and typically short deposition time (up to 20 min).

Plasma codeposition with stainless steel was used to form graded interfaces for strong adhesion of plasma polymers to stainless steel substrates. We used a reactive sputtering method, in which the cathode material was 316L stainless steel. The system has a long cathode (2 m) providing a wide variation in the angle of incidence of the depositing material in the vertical plane. The substrate holder was rotated to give a 180° range in the angle of incidence in the horizontal plane. This wide range of angles is important to ensure conformal coverage of complex-shaped objects, such as implantable prosthetic devices. Argon and acetylene were used in the process and were injected into the chamber through a distributed gas line with an array of holes at 10-cm intervals. The argon is used to achieve sputtering of the stainless steel with a target sputtering current controlled to be 3.2 A, and the acetylene is used to codeposit the plasma polymer. The voltage on the sputtering target varies from 700 to 400 V as the acetylene flow rate is increased.

During the deposition of the polymer-metal mixed films used to study the effect of stainless steel inclusions on covalent immobilization capability of the films, the flow of argon was automatically adjusted to maintain a total chamber pressure of 0.9 Pa when combined with the acetylene flow. Acetylene flow rates of 0, 10, 30, 40, 50, and 60 sccm were used in the deposition of the samples studied. The flow rate of argon is approximately 100 sccm when no acetylene is flowed into the chamber.

ESR measurements were carried out using a Bruker Elexsys E500 EPR spectrometer operating in X band with a microwave frequency of 9.33 GHz and a center field of 3,330 G, at room temperature. The spectrometer was calibrated using a weak pitch sample in KCl and also with DPPH (α,α′—diphenyl-β-picrylhydrazyl). PIII-treated polymer films, cut to a size of 5 cm × 5 cm, were rolled and placed into a quartz tube of 5-mm diameter. Typically, the films were 0.2-mm thick. The thinner 50-μm films of LDPE were rolled on a plastic needle. The spectrum of the tube with the plastic needle and without LDPE film was recorded before each measurement.

For analysis of plasma-polymerized coatings, the microwave frequency in the ESR analysis was 9.33 GHz, and microwave power was 1.975 mW. A 12-μm-thick polyimide foil was used as the substrate for the deposition of the plasma polymers for ESR measurements. The ESR analysis of plasma-polymerized samples was performed after approximately 24 h of storage in air.

Contact angle as a measure of wettability was measured using the sessile drop method on a Kruss contact angle analyzer DS10.

Deionized water, glycerol, methylene diiodine, and formamide were dropped onto the samples, and the angle between the edge of the drop and the surface was measured. The surface energy and its components (polar and dispersic parts) were calculated using the Owens–Wendt–Rabel–Kaelble model.

FTIR spectra were recorded using a Digilab FTS7000 FTIR spectrometer fitted with an ATR accessory (Harrick) with trapezium Germanium crystal and incidence angle of 45°. To obtain sufficient signal/noise ratio and resolution of spectral bands, we used 100–500 scans and a resolution of 1 cm^{-1}. The thickness of the measured layer was 400–800 nm depending on the wavenumber. Control samples (not subjected to incubation in protein solution) were incubated in buffer and washed in deionized milliQ water (mQ-water) at the same time as the samples with attached protein were undergoing the equivalent processes. The samples undergoing SDS treatment prior to FTIR measurement were immersed in SDS 2% solution in mQ-water for 1 h at 70 °C unless stated otherwise. After incubation in detergent, the samples were washed in mQ-water three times (for 20 min each time) at 23 °C. All samples were dried overnight, and ATR-FTIR spectra were recorded for protein attached and control samples on the same day. The intensity of the C=O group absorption was determined from the absorption intensity at 1,720 cm^{-1}. The peak intensity was normalized using the intensity of the 1,462 cm^{-1} methylene group vibration as internal standard. The amount of protein on surfaces was assessed according to the intensity of Amide A, I and II vibrations from the protein backbone.

The determination of the number and position of individual components of the amide I line to provide information related to the secondary structure of the protein was done by deconvolution of the spectra using the GRAMS software. To compare the structure of HRP attached to surfaces with native protein, we covered the germanium ATR crystal with a thick layer (some micrometers) of HRP, which had been dialyzed against water to remove salts, and allowed it to dry. Because the HRP layer is so thick, changes due to interactions of HRP with the surface of the germanium crystal have a negligible effect on the protein bands in the ATR-FTIR spectrum. The amide I band was fitted with Gaussian functions to represent the component peaks. During fitting, the variations of positions and widths of the component lines were constrained. The initial model, which was adjusted to achieve the best fit, was based on the results of second derivative, deconvolutions, and on literature data of peak positions, peak widths, and number of peaks (2–8). It included lines at 1,694, 1,684, and 1,674 cm^{-1} to represent vibrations in β-turns; at 1,661 and 1,649 cm^{-1} to represent vibrations in α-helices; at 1,635 cm^{-1} to represent vibrations in random structures; and at 1,623 cm^{-1} to represent vibrations in β-sheets. The integral intensity of component peaks was normalized and used to calculate the fractions of specific structures in the protein layer.

Atomic force microscopy (AFM) images of samples were collected on a PicoSPM instrument in tapping mode at a scan rate of 0.427 lines/s over an area of 1 μm × 1 μm. Analysis of the AFM images was performed using the WSxM software (version 3, Nanotec Electronica S.L.).

Ellipsometry (Woollam M2000V spectroscopic ellipsometer) was used to determine thicknesses and optical constants of PS films spun onto silicon wafers, before and after PIII treatment, and also after incubation in protein solution. Ellipsometric data were collected for three angles of incidence: 65, 70, and 75°. Cauchy layer models were used to fit the polymeric and protein layers. In the case of ion-treated samples, a Cauchy layer with absorption was required. The thickness and optical constants associated with the best-fit model were determined for each PS layer prior to protein incubation. These parameters were kept fixed for subsequent modeling of the protein layer after HRP was applied. In cases when the AFM images showed that there was a smooth surface, indicating complete coverage of the protein layer, a model consisting of separate Cauchy layers for the protein layer and the PS film on a silicon substrate was used to fit the data. However, when there was incomplete coverage of protein on the surface as shown by AFM, a Bruggeman effective medium approximation was used for the protein layer together with optical constants for the protein as determined from the complete coverage models. The parameters fitted for the protein layer were then only the thickness and void fraction.

Assays of HRP function were performed using tetramethylbenzidene (TMB) to assess the activity of HRP immobilized on the polymer surfaces. The treated polymer films and untreated controls were incubated with HRP within 2 weeks of venting the vacuum chamber to air. The HRP was from Sigma, catalog no. P6782. We used 10 mM PO_4 at pH 7 to dissolve the protein.

Unless otherwise stated, the HRP concentration in the buffer solution was 50 μg/mL. The protein concentration was verified by absorption from the heme group at 403 nm using the extinction coefficient of 102 mM cm^{-1}. After overnight incubation in the HRP buffer solution, samples were washed six times for 20 min in fresh buffer solution. Each wash involved rocking the samples floating face down in the fresh buffer solution. A set of untreated control samples was also incubated in the protein solution and then washed in the same way. After washing, each sample was clamped between two stainless steel plates separated by an O ring (inner diameter 8 mm; outer diameter 11 mm) that sealed to the sample surface. The top plate contained a 5-mm-diameter hole, enabling the addition of 75 μL of TMB (3,3′,5,5′ tetramethylbenzidine liquid substrate system for ELISA—Sigma T0440), an HRP substrate containing 0.012% hydrogen peroxide, to an area of polymer surface determined by the diameter of the O ring. After 30 s, 25-μL aliquots were taken and added to 50 μL of 2 M HCl in a 100-μL cuvette, and another 25 μL of TMB was added to bring the volume to 100 μL. The optical density (OD) at a wavelength of 450 nm was measured in transmission through the cuvette using a Beckman DU530 Life Science UV/vis spectrophotometer. Each data point presented was the average of measurements taken from at least three samples. To ensure that the OD measured in this HRP activity assay is not affected by chemical processes occurring on the buffer-soaked polymer surfaces, the assay is also conducted without HRP. In these cases, the OD reading was zero.

ELISA complemented infrared spectroscopy as a measure of tropoelastin coverage on surfaces. Strips of untreated and PIII-treated PTFE were cut into 0.8 cm × 1.2 cm rectangles and placed into the wells of a 24 well plate (Greiner). Tropoelastin was diluted to the appropriate concentration in PBS and 0.75 mL added per well and incubated under the specified conditions. Unbound tropoelastin was removed by aspiration, and the samples were washed with 3 × 1 mL aliquots of PBS. The samples undergoing SDS treatment prior to ELISA were transferred to 1.5 mL of 5% SDS (wt/vol) in PBS and incubated at 90 °C for 10 min. Nontreated samples were washed in 3 × 1 mL PBS at room temperature. The samples were returned to the 24 well plate and washed with 3 × 1 mL PBS. Nonspecific binding to the polymer was blocked with 3% (wt/vol) BSA in PBS for 1 h at room temperature. Following BSA blocking, the samples were washed with 2 × 1 mL PBS, then incubated in 0.75 mL of 1:2,000 diluted mouse antielastin antibody (BA-4) for 1 h at room temperature. The antibody was removed, and the samples were washed in 3 × 1 mL PBS before incubation in 0.75 mL of 1:10,000 diluted goat antimouse IgG-HRP conjugated secondary antibody for 1 h at room temperature. The secondary antibody was removed, and the samples were washed with 4 × 1 mL PBS. The samples were transferred to a new 24 well plate, and 0.75 mL ABTS solution (40 mM ABTS [2,2′-azino-bis (3-ethylbenzthiazoline-6-sulphonic acid)] in 0.1 M NaOAc, 0.05 M NaH_2PO_4, pH5, containing 0.01% (vol/vol) H_2O_2) was added. After 30–40 min, the plates were agitated and 100-μL

aliquots of the ABTS were transferred to a 96 well plate, and the absorbance was read at 405 nm using a plate reader. Thrombogenicity testing of blood components in static assays and of whole blood in a circulating flow system was carried out to compare the thrombogenicity of surfaces.

Whole blood was obtained using a 21G butterfly needle from healthy, nonsmoking, male volunteers with informed consent in accordance with the Declaration of Helsinki. Volunteers had not taken aspirin 2 weeks prior to donation. Approval for this work was granted by The University of Sydney, Human Research Ethics Committee (Reference no. 05-2009/11668).

Platelets were isolated from whole blood anticoagulation with acid citrate dextrose (9:1) and centrifuged for 15 min at $112 \times g$. The supernatant was further centrifuged for 10 min at $447 \times g$. The platelet pellet was resuspended in Tyrodes buffer and adjusted to 6×10^7 platelets/mL with saline. $CaCl_2$ and $MgCl_2$ were added to give final concentrations of 2.5 and 1 mM, respectively. Platelet-rich plasma (PRP) was obtained from whole blood anticoagulated with 0.5 U/mL heparin and centrifugation for 15 min at $112 \times g$. Wells of a 24 or 48 well plate were blocked with 3% BSA in saline for 30 min at room temperature and washed three times with saline. Isolated platelet suspension or PRP was incubated in wells containing 316L stainless steel sheet or ion-treated plasma polymer coated 316L stainless steel sheet samples at 37 °C for 30 min with rocking. Samples were processed for scanning electron microscopy (SEM) as described in ref. 9, or washed in d.H_2O and analyzed by ATR-FTIR. Modified Chandler loops were carried out with heparinized whole blood as previously described (9).

SI Results and Discussion

Detergent Washing as Evidence for Covalent Protein Immobilization. SDS is a detergent that is used to unfold proteins (10). SDS interferes with the physical forces that are responsible for the physisorption of proteins onto surfaces but does not attack covalent bonds, leaving the protein's primary structure intact. SDS washing has been used as a method to test whether biological molecules are covalently attached to surfaces (11–13) and to detect covalently bound drug–protein adducts (14). In some situations, steric hindrance may prevent the SDS from accessing all of the sites where physical forces bind the protein to the surface. An example of such a situation may occur where there is a thick coverage of strongly denatured and aggregated protein completely blocking access to the interface at the surface. Because our PIII-treated and plasma-deposited surfaces are relatively hydrophilic compared to untreated polymer controls from which our SDS wash successfully removes all of the protein, it is unlikely that steric hindrance could be responsible for the SDS-resistant binding observed on the PIII-treated surfaces. We therefore deduce that the high proportion of enzyme still adsorbed after SDS cleaning implies that our PIII-treated and plasma-deposited surfaces have sites capable of covalently binding protein. Covalent bonds between free radicals on the surface of a plasma-treated polymer and molecules in vapor are the basis of well-known plasma-assisted graft polymerization methods (15). Direct covalent immobilization of protein molecules has previously been observed on a range of PIII-treated polymers as well as for plasma-polymerized layers with similar surface chemistry and structure (16–24).

For all studies other than ELISA and unless stated otherwise, samples were immersed in SDS 2% solution in mQ-water for 1 h at 70 °C. After incubation in detergent and prior to FTIR measurement, the samples were washed in mQ-water three times (for 20 min each time) at 23 °C. In the case of ELISA measurements, 5% SDS (wt/vol) in PBS was used at 90 °C for 10 min. The samples were then returned to the 24 well plate and washed with 3×1 mL PBS. As shown in Fig. S1, typically both of these and other detergent washing protocols (as described in Table S1) removed more protein from the more hydrophobic untreated controls than they did from the relatively hydrophilic treated polymer surfaces, indicating the presence of covalently bound protein molecules. Variation of the protein amount on untreated polymer surfaces after detergent washing is likely to be caused by the variable history of the polymer samples. Data specifying the conditions of synthesis and storage before incubation is not typically available.

Derivation of a Kinetic Theory Model for Radical Quenching and Covalent Immobilization from Solution. Consider a reservoir of depth h containing unpaired electrons of number density n_r. A kinetic theory result for the time constant for decay of the unpaired electrons is obtained by considering the number of radicals decaying dN in time dt to be the number that is incident on the surface and quenched plus the number that react with each other in the bulk:

$$\frac{dN}{dt} = -A\frac{n_r \bar{\nu}_r S}{4} - KAhn_r^2, \qquad [S1]$$

where $\bar{\nu}_r$ is the mean velocity of the unpaired electrons in the reservoir, S is the quenching probability upon reaching the surface, A is the area of the surface, and K is a constant that depends on the cross-section for collisions between radicals in the bulk. Because $N = Ahn_r$, [**S1**] can be written

$$\frac{dn_r}{dt} = -\frac{n_r \bar{\nu}_r S}{4h} - Kn_r^2. \qquad [S2]$$

This differential equation has the solution

$$n_r = \left(\left(\frac{4hK}{\bar{\nu}_r S} + \frac{1}{n_0}\right)e^{\frac{\bar{\nu}_r St}{4h}} - \frac{4hK}{\bar{\nu}_r S}\right)^{-1}, \qquad [S3]$$

where n_0 is the unpaired electron number density at time, $t = 0$. In the case where surface recombination of radicals dominates over the bulk recombination, $K = 0$, and this equation reduces to

$$n_r = n_0 e^{-\frac{\bar{\nu}_r St}{4h}}, \qquad [S4]$$

which describes an exponential decay with time constant $\tau = \frac{4h}{\bar{\nu}_r S}$ and initial radical density of n_0. The relative importance of bulk and surface recombination was studied by fitting the data of Fig. 2*D* with both the three-parameter fit of [**S3**] with parameters K, τ, n_0, and the two-parameter fit of [**S4**] with parameters τ and n_0. Both [**S3**] and [**S4**] gave good fits to the data, with approximately the same R^2 of 0.967 and 0.953, respectively. However, the three-parameter fit did not give well-determined values of the fitting parameters, with the uncertainties in the parameter values exceeding the parameter values. Consequently, the two-parameter fit of [**S4**] was used. This choice is also preferred for physical reasons, because the recombination of free electrons at a surface where they are confined to move in two dimensions or are trapped is likely to be a more probable process than recombination in the bulk, which requires a collision in three-dimensional space with small cross-section. The large surface area compared to the small depth of the free radical reservoir means that the radicals have ready access to the surface and are therefore less likely to recombine in the bulk.

When the reservoir is created in an already formed polymer, the reservoir depth h depends on the ion energy used for implantation and the type of ion used, whereas when the reservoir is a polymer deposited from a plasma containing monomeric precursor during ion bombardment, the depth h is the thickness of the deposited layer. For typical values of h, the decay time of the unpaired electrons in the reservoir is long compared to times

of incubation in protein solution to achieve immobilization. Therefore, to determine an expression for the kinetics of protein immobilization from solution, we can assume a constant number density of unpaired electrons in the reservoir.

We now outline a mathematical description of the covalent attachment process in which radicals diffuse to the surface and form covalent bonds with physisorbed proteins. The first step is the physisorption of a protein on the surface, and the second step is the formation of a covalent bond between a protein residue and a radical group at the surface. There are two relevant time constants, one for the diffusion of proteins in solution to the surface and the second for the diffusion of the unpaired electrons from the reservoir to the surface. These processes are governed by the following two coupled differential equations:

$$\frac{dN_p}{dt} = \frac{(N_{\text{psites}} - N_p)}{\tau_1} \qquad \textbf{[S5]}$$

and

$$\frac{dN_C}{dt} = \frac{(FN_p - N_C)}{\tau_2}, \qquad \textbf{[S6]}$$

where N_p is the number of physisorbed protein molecules per unit area and N_c is the number of covalently immobilized protein molecules per unit area. τ_1 is the time constant for physical adsorption of molecules on the surface. τ_2 is the time constant for covalent immobilization of physically adsorbed molecules. N_{psites} is the number of sites available for physisorption per unit area, and F is the fraction of physisorption sites that are accessible to radicals diffusing from the interior reservoir. This set of equations has the following solutions:

$$N_p = N_{\text{psites}}(1 - e^{-t/\tau_1}) \qquad \textbf{[S7]}$$

and

$$N_C = FN_{\text{psites}}\left(1 - \frac{\tau_1 e^{-t/\tau_1}}{\tau_1 - \tau_2} - \frac{\tau_2 e^{-t/\tau_2}}{\tau_2 - \tau_1}\right). \qquad \textbf{[S8]}$$

Modeling the diffusion of molecules in solution as a Brownian motion gives the following for the physical adsorption time constant:

$$\tau_1 = \frac{4N_{\text{psites}}}{n_s \bar{\nu}_s S_s}, \qquad \textbf{[S9]}$$

where n_s is the number density of protein molecules in the solution, $\bar{\nu}_s$ is the mean velocity of their Brownian motion, and S_s is the probability that the molecules impinging on the surface from solution will be physically adsorbed.

Similarly, modeling the motion of unpaired electrons in the reservoir by kinetic theory gives the following equation for the time constant of covalent binding of adsorbed molecules, τ_2:

$$\tau_2 = \frac{4FN_{\text{psites}}}{n_r \bar{\nu}_r S_r}, \qquad \textbf{[S10]}$$

where n_r is the number density of unpaired electrons, $\bar{\nu}_r$ is the mean velocity associated with their diffusion, and S_r the probability of interaction with an adsorbed protein that forms a covalent bond.

Because the number density of free radicals in the reservoir beneath the surface decays with time, an increase in τ_2 for an aged sample is expected. The increase in τ_2 is expected to be greater than predicted on the basis of the reduction in n_r alone because both $\bar{\nu}_r$ and S_r may decrease with time. S_r would decrease as some of the surface becomes passivated by adsorption of atmospheric contaminants during storage. Radicals arriving at the surface at a site covered by contaminants will covalently bind to these rather than to a protein molecule. $\bar{\nu}_r$ may decrease because the unpaired electrons in environments allowing the highest mobility will have the highest rate of quenching.

In the case of plasma polymers deposited to different thicknesses under identical conditions, the density of unpaired electrons is constant throughout the layer. Thus,

$$\tau_2 = \frac{4FN_{\text{psites}}}{\bar{\nu}_r S_r n_r} = \frac{4FN_{\text{psites}}}{\bar{\nu}_r S_r n_0 \exp(-t_s/\tau)} = \frac{C}{\exp(-t_s/Bh)} \qquad \textbf{[S11]}$$

because $\tau = \frac{4h}{\bar{\nu}_r S}$. B and C are constants given by $C = \frac{4FN_{\text{psites}}}{\bar{\nu}_r S_r n_0}$ and $B = \frac{4}{\bar{\nu}_r S}$.

Substituting this into Eq. **S8** gives the following expression for the proportion of protein covalently coupled to a plasma polymer surface layer of thickness h, stored for time t_s after treatment and then incubated in protein for time t:

$$\frac{N_C}{FN_{\text{psites}}} = \frac{(\tau_1 - \tau_1 e^{t/\tau_1}) + \frac{C}{\exp(-t_s/Bh)}(e^{-t\exp(-t_s/Bh)/C} - 1)}{\tau_1 - \frac{C}{\exp(-t_s/Bh)}}. \qquad \textbf{[S12]}$$

The Importance of Unpaired Electron Mobility for Covalent Immobilization. Fig. S2 shows the effects of introducing structures that impede the mobility of unpaired electrons in the plasma polymer subsurface. Fig. S2*A* shows that the capability of the plasma polymer layer to covalently immobilize protein molecules is compromised by adding either oxygen or hydrogen to the hydrocarbon gas mix during the plasma polymerization process, while it is enhanced by the addition of nitrogen (25).

Hydrogen prevents the formation of unsaturated bonds between carbon atoms by forming sp^3 bonds with carbon so that the aromatic structures become divided by hydrocarbon groups. The plasma-deposited layer would then contain phenyl-like structures with methylene group bridges, with the latter becoming more dominant as the hydrogen concentration increases. The mobility of unpaired electrons along methylene bridges is roughly three orders of magnitude lower than in condensed aromatic ring structures (chapter 4 of ref. 26).

Oxygen atoms bond into condensed aromatic structures forming oxirene, oxete, furan, and pyrylium-like structures, which stabilize free radicals on conjugated π-electron clouds. The presence of oxygen in the carbon backbone outside the aromatic ring decreases the mobility of unpaired electrons along the chain. This is because a migrating unpaired electron will break the backbone at oxygen and form a carbonyl or hydroxyl group. The result is reduced mobility of unpaired electrons with the inclusion of oxygen (chapters 2 and 4 of ref. 27).

On the other hand, nitrogen atoms promote the formation of aromatic structures that provide high unpaired electron mobility. They bond with carbon, forming azirine, azete, pyrrole, and pyridine-like structures, where the valence electrons of nitrogen take part in sp^2hybridization. Such graphite-like structures form common π-electron clouds through the entire carbon region and stabilize active free radicals by the delocalization of the unpaired electrons. Nitrogen atom incorporation into the carbon backbone outside the condensed aromatic structures facilitates the migration of the unpaired electrons through the backbone while maintaining the backbone intact.

Fig. S2*B* shows the effect of codeposition of stainless steel with the plasma-deposited layer. The hydrocarbon component increases with increasing acetylene flow rate (indicated on the x axis), and this is strongly correlated with the amount of protein that is covalently attached after incubation in protein solution. An electron micrograph of one such layer codeposited with stain-

less steel is shown as an inset in the figure. The carbon rich components have been etched away using a hydrogen plasma. Therefore, the regions that were carbon rich appear light, whereas the stainless steel rich regions are dark. Free radicals cannot move into stainless steel, and the carbon regions of high mobility are interspersed by regions of steel, leading to reduced protein covalent binding capacity.

In the case of ion-implanted polymer surfaces, the ability to covalently attach protein molecules is also hampered by incorporation of structures that do not facilitate good unpaired electron mobility. For instance, virtually no covalent attachment is observed on PDMS or PEO after treatment with the same plasma immersion ion implantation process that produces excellent capacity for covalent attachment of proteins in polymers such as polyethylene, PS, and PTFE. Free radicals are observed, but they are of a different kind. Fig. S3*A* shows ESR data obtained from low density polyethylene (red), and PDMS (blue) after PIII treatment. Low-density polyethylene clearly has the highest density of unpaired electrons. Fig. S3*B* shows the integrated signal (black line) obtained from the PDMS ESR data fitted with peaks at the *g* factors associated with the local chemical environment of the unpaired electron. The composite peak is fitted well with separate Gaussian peaks at each *g* value. Unlike in LDPE ($C^* = 6.07 \times 10^{18}$ cm^{-3}), the signal is not dominated by unpaired electrons associated with C atoms but shows that the majority of unpaired electrons are associated with Si-O and Si ($C^* = 0.04 \times 10^{18}$ cm^{-3}; $Si^* = 0.18 \times 10^{18}$ cm^{-3}; $SiO^* = 0.17 \times 10^{18}$ cm^{-3}). In contrast to the hydrocarbon polymers, which form carbon-dominated structures after modification, the PIII-modified PDMS contains high concentrations of silicon and oxygen and hence structures that do not facilitate the transfer of free radicals from the bulk to the top surface. Because the majority of unpaired electrons are associated with Si and Si-O, they would not be expected to be mobile.

Covalent immobilization of proteins on PIII-treated PDMS-containing block copolymers is observed when there is a significant fraction of a carbon-rich polymer present. One such polymer is Elast-Eon™, a block copolymer of PDMS and polyurethane. Fig. S4 shows the dependence of the percentage of protein covalently attached as a function of the PIII treatment time. During PIII treatment, the acceleration of ions from a nitrogen plasma to the sample holder was achieved using pulses of 20-kV voltage, 10-μs duration at a frequency of 52 Hz. Treatment times were 10, 20, 40, 80, 180, 420, 520, 620, and 800 s. Superimposed on this data is the ESR signal measuring the free radical content for times up to 180 s and the concentration of carbon in the implanted structure, as measured by XPS, for times above 180 s. The proportion of covalently attached tropoelastin increases for PIII times up to 180 s. Above 180 s, although the ESR signal continues to increase (reaching 130,000 after 420 s of treatement), the fraction of the amount of protein covalently attached decreases. XPS measurements of the surface of the polymer showed that its composition changed steadily during the PIII treatment. Over the treatment time of 820 s, C decreased from 64 at% to 28 at%, O increased from 20 at% to 47 at%, Si increased from 13 at % to 20 at% while N remained between 3 at% and 6 at%. The decrease in the covalent attachment of protein is correlated with a decrease in the carbon concentration and simultaneous increases in the Si and O relative contents. Although the concentration of free radicals remains high for long treatment times, the changes in chemical composition have resulted in reductions in the mobility of the free radicals.

Universality of Covalent Immobilization Across Amino Acids. The chemical activity of the protein-binding free radicals appears to be universal with respect to amino acid side-chain groups. We conducted experiments on the covalent attachment of polyamino acids, which showed that most polyamino acids are covalently bound on incubation with the PIII-treated surface. Table S2 shows the poly-l-amino acids used, their side-chain terminal groups, and whether covalent binding was observed. All of the polyamino acids tested except glutamic acid showed SDS-resistant covalent attachment to the ion-treated polymer. The lack of attachment of poly-l-glutamic acid may be caused by repulsive electrostatic interactions or high hyrophilicity preventing initial adsorption on the surface. Because our surface layers are oxidized, it is possible that like charges form on the surface and the poly-l-glutamic acid resulting in repulsion on approach.

These data suggest that the chemical bonds between protein molecules and the carbonized surfaces can be formed through a variety of amino acids and thus are likely to occur for most protein molecules. An XPS study of the sulfur peaks associated with cystine amino acids in the protein, microperoxidase-11 (MP11), after surface attachment and then after SDS washing revealed that a particular chemical shift was associated with one cystine of the two in the protein for all covalently attached protein (28). This chemical shift is consistent with that of the sulfur valency electrons in S—O bonds. This may be an indication that in some cases ambient oxygen may participate in the covalent attachment. However, another experiment in which we incubated a freshly treated polymer surface in catalase solution without exposure to ambient showed strong covalent attachment, implying that the reactions can also proceeded without the involvement of ambient oxygen.

Fig. S5 shows SDS-resistant covalent attachment of catalase to PIII-treated polyethylene surfaces before and after exposure to air compared with that of untreated polyethylene and a block copolymer with high levels of surface oxygen. After contact with oxygen in air, the PIII-treated polymer contains peroxide and oxygen radicals. High levels of SDS-resistant attachment are observed on the PIII-treated samples, whereas the highly oxygenated surface of the block copolymer showed none. The sample incubated in catalase without exposure to air showed a high level of covalent protein attachment but lower levels of protein activity, indicating that multiple attachment expected according to the high concentrations of free radicals in the unpassivated sample may be binding the protein at too many sites to allow good functionality.

Blockers for Suppression of Covalent Immobilization. The covalent binding capacity of the interlayers can be reduced dramatically by incubation with chemical blockers capable of passivation of free radicals. The results of studies performed using a number of blocker molecules are shown in Fig. S6. UHMWPE films were PIII-treated with 10-kV, 20-μs pulses at 100 Hz for 18 min to give a fluence of 1×10^{16} ions/cm^{-2}. Two weeks after treatment, incubation was carried out in blocker solutions as described in Table S3. The presence of the blockers was confirmed by ATR-FTIR after rinsing and/or drying as described in Table S3. This was followed by incubation in 50 μg/mL HRP solution in PBS buffer overnight. After six washes in fresh buffer, the samples were analyzed with ATR-FTIR both before and after SDS washing. The results show that both TEMPO and benzylmercaptan reduce the covalent binding capacity of the PIII-treated polymer, whereas hexene and styrene do not. The TEMPO free radical and the active –SH group in benzylmercaptan both react with free radicals, removing them from the system while the active double-bond monomers such as hexene and styrene cause graft-copolymerization of the monomer layer on the PIII-treated surface. The bonding in this case is accommodated by opening the carbon double bonds with the result that free radicals on the attached molecule are created. The new free radical is also capable of forming covalent bonds with protein side chains, so these molecules may be acting as linkers rather than blockers.

1. Wu WJ, Vrhovski B, Weiss AS (1999) Glycosaminoglycans mediate the coacervation of human tropoelastin through dominant charge interactions involving lysine side chains. *J Biol Chem* 274:21719–21724.
2. Chen J, Xia C, Niu J, Li S (2001) FTIR study of horseradish peroxidase in reverse micelles. *Biochem Biophys Res Commun* 282:1220–1223.
3. Smeller L, Meersman F, Fidy J, Heremans K (2003) High-pressure FTIR study of the stability of horseradish peroxidase. Effect of heme substitution, ligand binding, Ca++ removal, and reduction of the disulfide bonds. *Biochemistry* 42:553–561.
4. Maeda Y, Fujihara M, Ikeda I (2002) Spectroscopic study on structure of horseradish peroxidase in water and dimethyl sulfoxide mixture. *Biopolymers* 67:107–112.
5. Al-Azzam W, *et al.* (2002) Structure of poly(ethylene glycol)-modified horseradish peroxidase in organic solvents: Infrared amide I spectral changes upon protein dehydration are largely caused by protein structural changes and not by water removal per se. *Biophys J* 83:3637–3651.
6. Sirotkin VA (2005) Effect of dioxane on the structure and hydration-dehydration of alpha-chymotrypsin as measured by FTIR spectroscopy. *Biochim Biophys Acta* 1750:17–29.
7. Schmidt TF, Caseli L, Viitala T, Oliveira ON, Jr. (2008) Enhanced activity of horseradish peroxidase in Langmuir-Blodgett films of phospholipids. *Biochim Biophys Acta* 1778:2291–2297.
8. Kondyurin A, Nosworthy NJ, Bilek MMM (2011) Effect of low molecular weight additives on immobilization strength, activity, and conformation of protein immobilized on PVC and UHMWPE. *Langmuir* 27:6138–6148.
9. Waterhouse A, et al. (2010) The immobilization of recombinant human tropoelastin on metals using a plasma-activated coating to improve the biocompatibility of coronary stents. *Biomaterials* 31:8332–8340.
10. Laemmli UK (1970) Cleavage of structural proteins during the assembly of the head of bacteriophage T4. *Nature* 227:680–685.
11. Shlyakhtenko LS, Gall AA, Weimer JJ, Hawn DD, Lyubchenko YL (1999) Atomic force microscopy imaging of DNA covalently immobilized on a functionalized mica substrate. *Biophys J* 77:568–576.
12. Vandenberg E, Elwing H, Askendal A, Lundstrom I (1991) Protein immobilization to 3-aminopropyl triethoxy silane/glutaraldehyde surfaces: Characterization by detergent washing. *J Colloid Interface Sci* 143:327–335.
13. Hodneland CD, Lee Y-S, Min D-H, Mrksich M (2002) Selective immobilization of proteins to self-assembled monolayers presenting active site-directed capture ligands. *Proc Natl Acad Sci USA* 99:5048–5052.
14. Zhou S (2003) Separation and detection methods for covalent drug-protein adducts. *J Chromatogr B Analyt Technol Biomed Life Sci* 797:63–90.
15. Ikada Y (1994) Surface modification of polymers for medical applications. *Biomaterials* 15:725–736.
16. Yin YB, et al. (2009) Plasma polymer surfaces compatible with a CMOS process for direct covalent enzyme immobilization. *Plasma Process Polym* 6:68–75.
17. Yin Y, et al. (2009) Acetylene plasma coated surfaces for covalent immobilization of proteins. *Thin Solid Films* 517:5343–5346.
18. Kondyurin A, Nosworthy NJ, Bilek MMM (2008) Attachment of horseradish peroxidase to polytetrafluorethylene (teflon) after plasma immersion ion implantation. *Acta Biomater* 4:1218–1225.
19. Kondyurin A, et al. (2008) Covalent attachment and bioactivity of horseradish peroxidase on plasma-polymerized hexane coatings. *Plasma Process Polym* 5:727–736.
20. Ho JPY, et al. (2007) Plasma-treated polyethylene surfaces for improved binding of active protein. *Plasma Process Polym* 4:583–590.
21. Bax DV, McKenzie DR, Weiss AS, Bilek MMM (2009) Linker-free covalent attachment of the extracellular matrix protein tropoelastin to a polymer surface for directed cell spreading. *Acta Biomater* 5:3371–3381.
22. Nojiri C, Senshu K, Okano T (1995) Nonthrombogenic polymer vascular prosthesis. *Artif Organs* 19:32–38.
23. Ganapathy R, Manolache S, Sarmadi M, Denes F (2001) Immobilization of papain on cold-plasma functionalized polyethylene and glass surfaces. *J Biomater Sci Polym Ed* 12:1027–1049.
24. Kondyurin A, Naseri P, Fisher K, McKenzie DR, Bilek MMM (2009) Mechanisms for surface energy changes observed in plasma immersion ion implanted polyethylene: The roles of free radicals and oxygen-containing groups. *Polym Degrad Stab* 94:638–646.
25. Yin YB, et al. (2009) Covalently bound biomimetic layers on plasma polymers with graded metallic interfaces for in vivo implants. *Plasma Process Polym* 6:658–666.
26. Emanuel NM, Buchachenko AL (1987) *Chemical Physics of Polymer Degradation and Stabilization* (VNU Science Press, Utrecht, The Netherlands).
27. Rabek JF (1995) *Polymer Photodegradation* (Chapman and Hall, London), p 664.
28. Yin Y, Bilek MMM, McKenzie DR (2010) Direct evidence of covalent immobilisation of microperoxidase-11 on plasma polymer surfaces. *Plasma Process Polym* 7:708–714.

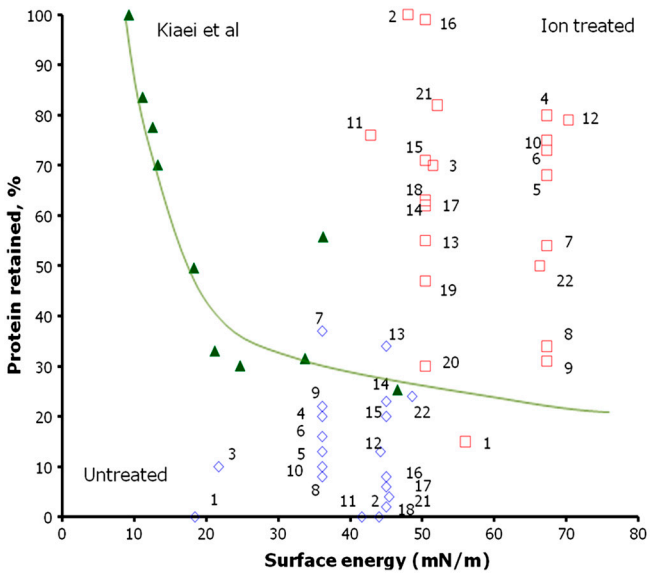

Fig. S1. Percent of protein retained after SDS washing (various solution strengths and temperatures) as a function of surface energy for various polymeric surfaces. Data is taken from Kiaei et al. (1) (green triangles) and current work (red squares and blue diamonds). Points (red squares and one green triangle) lying above and to the right of the trend curve typical for physically adsorbed protein show exceptional protein retention given the hydrophilic nature of these surfaces. Untreated controls washed with stronger SDS protocols than in Kiaei et al. are shown as blue diamonds. The polymer materials used and protocols for surface treatment, protein incubation, rinsing, and detergent washing are given in Table S1 in the row numbered as the data points. Two points are shown for each experiment number: The red square shows the result for the ion-treated polymer, whereas the blue diamond shows the result for the corresponding untreated control sample subjected to the same processing except for the ion treatment.

1 Kiaei D, Hoffman AS, Horbett TA (1992) Tight binding of albumin to glow discharge treated polymers. *J Biomater Sci Polym Ed* 4:35–44.

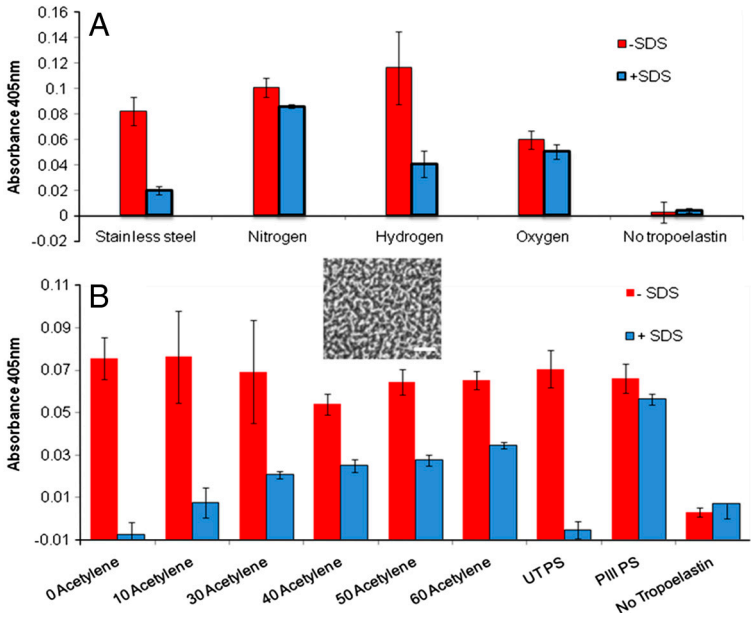

Fig. S2. (*A*) The effect on the covalent protein binding capacity of introducing nitrogen, hydrogen, and oxygen into the argon–acetylene gas mix during deposition from an acetylene precursor. Data for a stainless steel sheet and for the ELISA carried out in the absence of tropoelastin are shown as controls. (*B*) The effect of varying fractions of stainless steel inclusions on the covalent protein binding capacity of plasma-deposited films. Stainless steel was deposited together with a carbon containing plasma polymer from the precursor acetylene at a range of acetylene flow rates as indicated in sccm (first six points from left). Untreated and PIII-treated polystyrene are used as controls. The last data point shows absorbance values given by the assay in the absence of tropoelastin. The inset is an SEM image of the stainless steel after selectively etching back the plasma polymer layer in a hydrogen plasma. Scale bar, 100 nm.

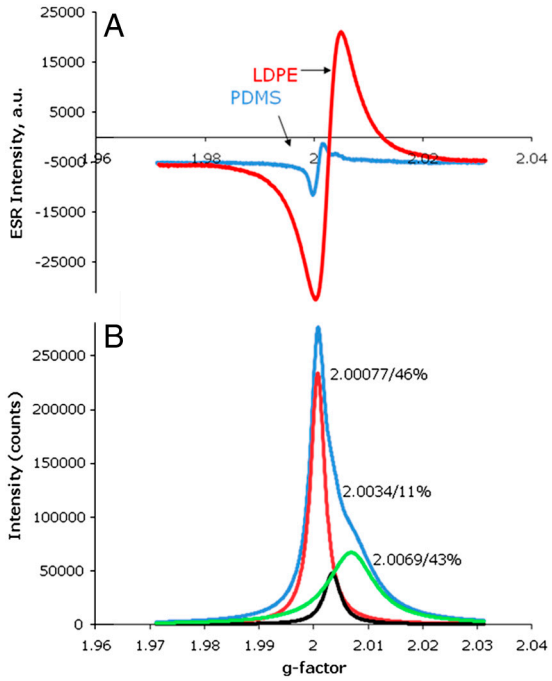

Fig. S3. (*A*) ESR spectra of PIII-treated LDPE (red) and PDMS (blue). (*B*) ESR spectrum of PIII-treated PDMS (blue) fitted according to *g*-factor shifts. Fitting the composite curve by Gaussian peaks associated with *g* values for unpaired electrons on C, Si-O, and Si gives the proportions shown [$C^* = 0.04 \times 10^{18}$ cm^{-3} (black); $Si^* = 0.17 \times 10^{18}$ cm^{-3} (green); $Si\text{-}O^* = 0.18 \times 10^{18}$ cm^{-3} (red)]. The unpaired electrons on carbon atoms are in the minority and have a very small concentration compared to those in LDPE ($C^* = 6.07 \times 10^{18}$ cm^{-3}).

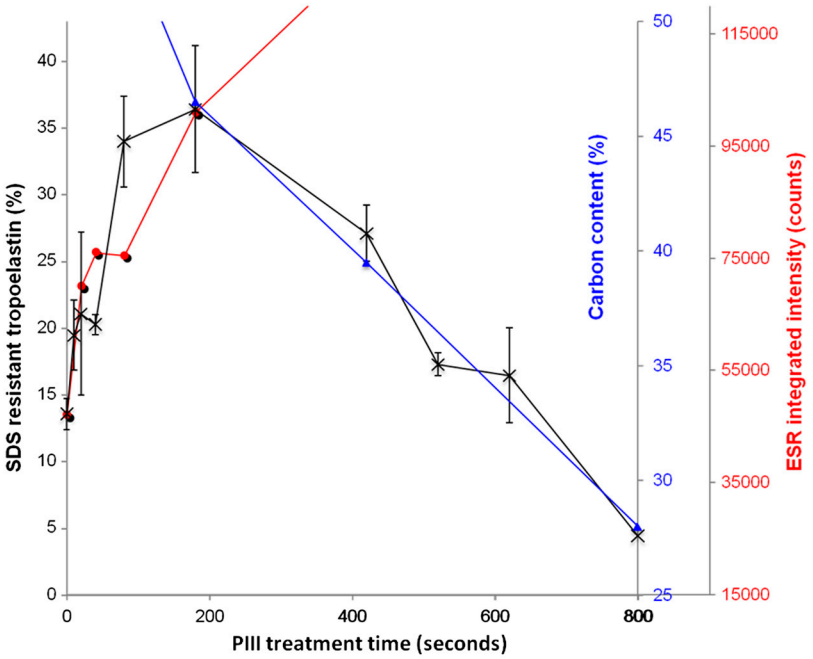

Fig. S4. SDS-resistant immobilization (black crosses) on PIII-treated Elast-Eon™ measured by the ratio of ELISA signals with and without SDS washing plotted as a function of treatment time. Initially, an increase in SDS-resistant immobilization correlated with the increase in the ESR integrated intensity (red circles) is observed. For treatment times beyond 200 s, however, the SDS-resistant immobilization falls despite the fact that the ESR integrated intensity continues to rise. This fall is correlated with a decrease in the carbon content (blue triangles) of the polymer. Carbon is more easily sputtered from the surface than silicon, so the relative concentration of carbon falls with treatment time.

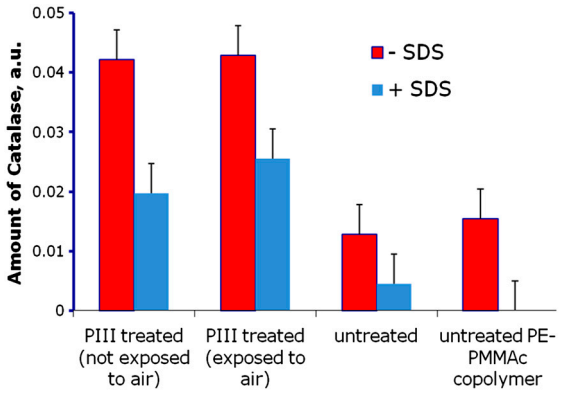

Fig. S5. Amount of catalase as measured by ATR-FTIR with (blue bars) and without (red bars) SDS detergent washing. Surfaces incubated in catalase solution are (from left to right) PIII-treated UHMWPE not exposed to air prior to incubation with the protein, PIII-treated UHMWPE exposed to air prior to incubation with the protein, untreated UHMWPE, and an untreated copolymer of polyethylene and polyacrylyc acid.

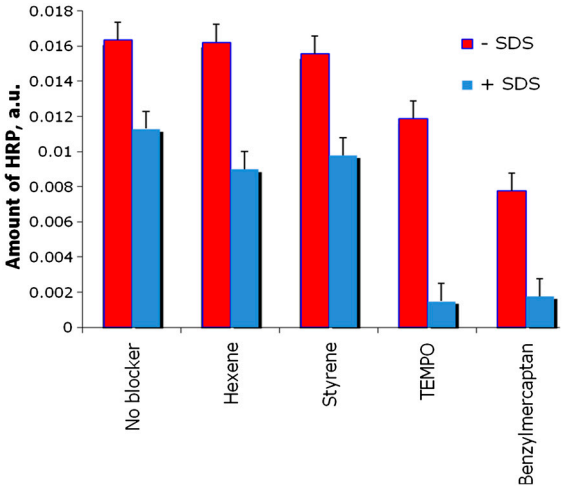

Fig. S6. HRP amount (measured using ATR-FTIR spectroscopy) on PIII-treated UHMWPE with (blue) and without (red) SDS washing after incubation. The surfaces were incubated in various chemical blockers (from left to right—none, hexene, styrene, TEMPO, and benzylmercaptan) and subsequently rinsed prior to incubation in HRP solution for protein immobilization. The presence of the blockers on the UHMWPE surface was confirmed using ATR-FTIR spectroscopy prior to incubation in the HRP solution.

Table S1. Details of polymer materials, PIII treatment, protein incubation, rinsing, and detergent washing protocols for all data labeled with a measurement number (open symbols) in Fig. S1

Measurement number/type (Fig. S1)	Polymer material	Treatment time (fluence), time until protein incubation	Incubation in protein solution	Rinsing protocol	Detergent washing protocol
1 FTIR data	PDMS, 1-mm sheet, cast from toluene and cured	800 s (1e16 ions/cm^2), 2 weeks	50 μg/mL tropoelastin in PBS, incubated overnight at RT	six PBS washes	2% SDS for 1 h at 70 °C
2 FTIR data	Polypyrrole, electrodeposited on gold-PET substrate	20 s (2.5e14 ions/cm^2), 2 weeks	50 μg/mL tropoelastin in PBS, incubated overnight at RT	six PBS washes	2% SDS for 1 h at 70 °C
3 FTIR data	PTFE, film of 0.025-mm thickness from Halogen (Perm)	800 s (1e16 ions/cm^2), 1 mo	50 μg/mL HRP in PO_4 buffer, incubated overnight at RT	six PO_4 buffer washes	2% SDS for 1 h at 70 °C
4 FTIR data	LDPE, film of 0.02-mm thickness from Goodfellow	800 s (1e16 ions/cm^2), 2 weeks	50 μg/mL HRP in PO_4 buffer, incubated overnight at RT	six PO_4 buffer washes	2% SDS for 1 h at 70 °C
5 FTIR data	UHMWPE, 0.2-mm sheets from Goodfellow	800 s (1e16 ions/cm^2), 2 weeks	50 μg/mL HRP in PO_4 buffer, incubated overnight at RT	six PO_4 buffer washes	2% SDS for 1 h at 70 °C
6 FTIR data	UHMWPE, 0.2-mm sheets from Goodfellow	800 s (1e16 ions/cm^2), 2 weeks	50 μg/mL BSA in PO_4 buffer, incubated overnight at RT	six PO_4 buffer washes	2% SDS for 1 h at 70 °C
7 FTIR data	UHMWPE, 0.2-mm sheets from Goodfellow	800 s (1e16 ions/cm^2), 2 weeks	50 μg/mL ovalbumin in PO_4 buffer, incubated overnight at RT	six PO_4 buffer washes	2% SDS for 1 h at 70 °C
8 FTIR data	UHMWPE, 0.2-mm sheets from Goodfellow	800 s (1e16 ions/cm^2), 2 weeks	50 μg/mL ovalbumin in PO_4 buffer, incubated overnight at RT	six PO_4 buffer washes	2% SDS for 1 h at 70 °C followed by 1% DTT for 20 min at RT
9 FTIR data	UHMWPE, 0.2-mm sheets from Goodfellow	800 s (1e16 ions/cm^2), 2 weeks	50 μg/mL ribonuclease in PO_4 buffer, incubated overnight at RT	six PO_4 buffer washes	2% SDS for 1 h at 70 °C
10 FTIR data	UHMWPE, 0.2-mm sheets from Goodfellow	800 s (1e16 ions/cm^2), 2 weeks	50 μg/mL BMP-7 in PBS, incubated overnight at RT	six PBS washes	2% SDS for 1 h at 70 °C
11 FTIR data	PMMA sheets cast from acetone/ethylacetate solution, thickness of 0.3 mm	800 s (1e16 ions/cm^2), 2 weeks	50 μg/mL HRP in PO_4 buffer, incubated overnight at RT	six PO_4 buffer washes	2% SDS for 1 h at 50 °C
12 XPS data, on intensity of sulfur 2p peak	nylon	1,600 s (2e16 ions/cm^2), 1 y	50 μg/mL HRP in PO_4 buffer, incubated overnight at RT	six PO_4 buffer washes	2% SDS for 1 h at 70 °C
13 FTIR data	PS, 0.25-mm sheets, from Goodfellow	1,600 s (2e16 ions/cm^2), 1 mo	50 μg/mL HRP in PO_4 buffer, incubated overnight at RT	six PO_4 buffer washes	2% SDS for 1 h at 23 °C
14 FTIR data	PS, 0.25-mm sheets, from Goodfellow	1,600 s (2e16 ions/cm^2), 1 mo	50 μg/mL HRP in PO_4 buffer, incubated overnight at RT	six PO_4 buffer washes	2% SDS for 1 h at 40 °C
15 FTIR data	PS, 0.25-mm sheets, from Goodfellow	1,600 s (2e16 ions/cm^2), 1 mo	50 μg/mL HRP in PO_4 buffer, incubated overnight at RT	six PO_4 buffer washes	2% SDS for 1 h at 100 °C
16 FTIR data	PS, 0.25-mm sheets, from Goodfellow	1,600 s (2e16 ions/cm^2), 1 mo	50 μg/mL HRP in PO_4PO_4 buffer, incubated overnight at RT	six PO_4 buffer washes	2% Triton for 1 h at 23 °C
17 FTIR data	PS, 0.25-mm sheets, from Goodfellow	1,600 s (2e16 ions/cm^2), 1 mo	50 μg/mL HRP in PO_4 buffer, incubated overnight at RT	six PO_4 buffer washes	2% Triton for 1 h at 40 °C
18 FTIR data	PS, 0.25-mm sheets, from Goodfellow	1,600 s (2e16 ions/cm^2), 1 mo	50 μg/mL HRP in PO_4 buffer, incubated overnight at RT	six PO_4 buffer washes	2% Triton for 1 h at 70 °C
19 FTIR data,	PS, 0.25-mm sheets, from Goodfellow	800 s (1e16 ions/cm^2), 2 weeks	50 μg/mL soybean peroxidase in PO_4 buffer, incubated overnight at RT	six PO_4 buffer washes	2% SDS for 1 h at 70 °C
20 FTIR data	PS, 0.25-mm sheets, from Goodfellow	800 s (1e16 ions/cm^2), 2 weeks	50 μg/mL soybean peroxidase in PO_4 buffer, boiled for 1 h	six PO_4 buffer washes	2% SDS for 1 h at 70 °C
21, FTIR data	PVC without plastisizer, 0.2-mm sheets, from Goodfellow	800 s (1e16 ions/cm^2), 2 weeks	50 μg/mL HRP in PO_4 buffer, incubated overnight at RT	six PO_4 buffer washes	2% SDS for 1 h at 70 °C
22 FTIR data	PES, 0.025-mm film, from Goodfellow	80 s (1e15 ions/cm^2), 3 weeks	50 μg/mL HRP in PO_4 buffer, incubated overnight at RT	six PO_4 buffer washes	2% SDS for 1 h at 70 °C

The measurement number is shown in the first column, and the PIII treatment was carried out in nitrogen plasma using 20-kV pulses of 20-μs length, applied at 50 Hz in all cases. RT, room temperature; BMP-7, bone morphogenic protein-7.

Table S2. Covalent attachment of polyamino acids on PIII-treated polyethylene

Amino acid	Polyamino acid and solvents used	Chemical side-chain groups present	Covalent attachment to PIII-treated PE
Glycine (Gly, G)	polyglycine $M_r = 1{,}400$ (from PBS buffer pH12; from acetone)	$-CH_2-$	yes, yes
Alanine (Ala, A)	polyalanine (from water; from acetone)		yes, yes
Isoleucine (Iso, I)	polyisoleucine (from acetone)		yes
Proline (Pro, P)	polyproline (from acetone)		yes
Lysine (Lys, K)	poly-l-lysine $M_r = 30{,}000$ (from PBS buffer pH7)	$-CH_2-$	yes
Arginine (ARG, R)	polyarginine (from TFA-MSA water solution)	$-NH_2$	yes
Histidine (His, H)	poly-l-histidine (from PBS buffer pH6; from acetone)	—NH— =N— —CH=	yes, yes
Tryptophan (Trp, W)	poly-l-tryptophan $M_r = 18{,}200$ (from acetone)	—NH— —CH=	yes
Tyrosine (Try, Y)	poly-l-tyrosine $M_r = 40{,}000$ (from acetone)	—OH	yes
Threonine (Thr, T)	polythreonine (from water; from acetone)		yes
Glutamic acid (Glu, E)	poly-l-glutamic acid, $M_r = 14{,}500$ (from PBS buffer pH7)	—COOH	no
Methionine (Met, M)	polymethionine (from acetone)	$-CH_2-$ —SH	yes

PE, polyethylene; TFA-MSA, trifluoroacetic acid and methanesulfonic acid.

Table S3. Reagents trialed as chemical blockers of covalent immobilization capability on PIII-treated UHMWPE surfaces

Blocker molecule	Solvent	Removal of residual blocker
Hexene	hexane, 30%	drying
Styrene	toluene, 30%	drying
TEMPO	acetone, 10% wt/wt	washing in acetone
Benzylmercaptan	toluene, 30%	washing in toluene and drying

The blockers listed were applied by overnight incubation in the solutions with the solvents indicated after removal of UHMWPE samples from the PIII treatment chamber. After blocking, the samples were washed and/or dried (as indicated) to remove nonbonded blocker molecules.